Acta Crystallographica Section D
Biological Crystallography
ISSN 0907-4449

Heat transfer from protein crystals: implications for flash-cooling and X-ray beam heating

S. Kriminski,[a] M. Kazmierczak[b] and R. E. Thorne[a]*

[a]Laboratory of Atomic and Solid State Physics, Cornell University, Ithaca, NY 14853, USA, and [b]Department of Mechanical Engineering, University of Cincinnati, Cincinnati, OH 45221, USA

Correspondence e-mail: ret6@cornell.edu

Received 18 October 2002
Accepted 31 January 2003

Three problems involving heat transfer from a protein crystal to a cooling agent are analyzed: flash-cooling in a cold nitrogen- or helium-gas stream, plunge-cooling into liquid nitrogen, propane or ethane and crystal heating in a cold gas stream owing to X-ray absorption. Heat transfer occurs by conduction inside the crystal and by convection from the crystal's outer surface to the cooling fluid. For flash-cooling in cold gas streams, heat transfer is limited by the rate of external convection; internal temperature gradients and crystal strains during cooling are very small. Helium gas provides only a threefold improvement in cooling rates relative to nitrogen because its much larger thermal conductivity is offset by its larger kinematic viscosity. Characteristic cooling times vary with crystal size L as $L^{3/2}$ and theoretical estimates of these times are consistent with experiments. Plunge-cooling into liquid cryogens, which can give much smaller convective thermal resistances provided that surface boiling is eliminated, can increase cooling rates by more than an order of magnitude. However, the internal conduction resistance is no longer negligible, producing much larger internal temperature gradients and strains that may damage larger crystals. Based on this analysis, factors affecting the success of flash-cooling experiments can be ordered from most to least important as follows: (1) crystal solvent content and solvent composition, (2) crystal size and shape, (3) amount of residual liquid around the crystal, (4) cooling method (liquid plunge *versus* gas stream), (5) choice of gas/liquid and (6) relative speed between cooling fluid and crystal. Crystal heating by X-ray absorption on present high-flux beamlines should be small. For a fixed flux and illuminated area, heating can be reduced by using crystals with areas normal to the beam that are much larger than the beam area.

1. Introduction

X-ray data collection from biomacromolecular crystals is usually performed at cryogenic temperatures in order to minimize radiation damage (Hope, 1990; Rodgers, 1994; Chayen *et al.*, 1996; Garman & Schneider, 1997; Garman, 1999). Slow cooling allows water inside and surrounding the crystal to form hexagonal ice, disrupting the order of the protein lattice and creating ice rings that obscure its diffraction (Weik *et al.*, 2001). Additional disorder may result from relaxation of protein conformation (Young *et al.*, 1991) and from differential expansion of the protein lattice and solvent (Juers & Matthews, 2001; Kriminski *et al.*, 2002). Rapid or 'flash' cooling a crystal to below water's glass transition at $T_g \simeq 140$ K can freeze water into an amorphous (vitreous) form (Barkalov *et al.*, 1993; Sartor *et al.*, 1994) and prevent its

Table 1
Density ρ, heat capacity per unit mass c_p, viscosity η, thermal conductivity κ, kinematic viscosity ν, thermal diffusivity χ and Prandtl number Pr of nitrogen and helium gas and of liquid nitrogen, propane and ethane at selected temperatures.

Properties of gases are taken at 0.1 MPa. Ambient pressure boiling temperatures for liquid nitrogen, ethane and propane are 77, 185 and 231 K, respectively; parameter values at higher temperatures are for pressurized liquids. For nitrogen, which has a critical temperature of 126 K (Rah & Eu, 2001), the liquid data are given at 10 MPa, roughly three times the critical pressure of 3.4 MPa (Lide, 2000).

	ρ (kg m^{-3})	c_p (J g^{-1} K^{-1})	η (μPa s)	κ (W m^{-1} K^{-1})	ν (10^{-6} m^2 s^{-1})	χ (10^{-6} m^2 s^{-1})	Pr
N_2 (g)							
100 K	3.5†	1.0†	6.8†	9.8×10^{-3}†	1.9	2.8	0.69
200 K	1.7†	1.0†	13†	1.9×10^{-2}†	7.6	11	0.69
300 K	1.2†	1.0†	18†	2.6×10^{-2}†	15	22	0.69
He (g)							
30 K	1.6‡	5.2‡	4.6‡	3.6×10^{-2}‡	2.9	4.3	0.65
100 K	0.48†	5.2‡	9.7†	7.6×10^{-2}†	20	30	0.65
200 K	0.24†	5.2†	15†	1.2×10^{-1}†	64	96	0.65
300 K	0.16†	5.2†	20†	1.6×10^{-1}†	1.3×10^{2}	1.9×10^{2}	0.65
N_2 (l)							
63 K	8.7×10^{2}†	1.5†	2×10^{2}§	0.15†	0.23	0.12	2.0
100 K	7.3×10^{2}†	1.6†	70†	0.11†	9.6×10^{-2}	9.4×10^{-2}	1.0
200 K	2.0×10^{2}†	1.3†	18†	3.0×10^{-2}†	9.2×10^{-2}	0.12	0.8
300 K	1.1×10^{2}†	0.9†	20†	3.2×10^{-2}†	0.18	0.32	0.6
C_2H_6 (l)							
90 K	6.5×10^{2}¶	2.3¶	1.1×10^{3}¶	0.24¶	1.6	0.16	10
100 K	6.3×10^{2}¶	2.3¶	9.3×10^{2}¶	0.23¶	1.5	0.16	9
200 K	5.6×10^{2}¶	2.4¶	1.9×10^{2}¶	0.15¶	0.23	0.12	2.0
273 K	4.0×10^{2}¶	3.5¶	65¶	9.5×10^{-2}¶	0.16	6.8×10^{-2}	2.4
C_3H_8 (l)							
86 K	7.3×10^{2}¶	1.9¶	9.5×10^{3}¶	0.21¶	13	0.15	90
100 K	7.2×10^{2}¶	1.9¶	4.5×10^{3}¶	0.21¶	6.3	0.15	40
200 K	6.2×10^{2}¶	2.2¶	3.0×10^{2}¶	0.15¶	0.48	0.11	4
300 K	4.9×10^{2}¶	2.7¶	1.1×10^{2}¶	9.2×10^{-2}¶	0.22	7.0×10^{-2}	3.2

† Taken from Lide (2000). ‡ Calculated based on data for He at higher temperatures and known physical laws. § Taken from Rah & Eu (2001). ¶ Taken from Gallian & Yaws (1992).

redistribution within the crystal and generally yields the best diffraction results.

Flash-cooling protocols can be optimized *via* at least two different routes: (i) by increasing cooling rates and/or (ii) by decreasing the cooling rates required to achieve vitrification of internal and external solvent. Transforming pure water to amorphous ice requires cooling from room temperature to below T_g in less than 10^{-4} s (Bruggeller & Mayer, 1980; Mayer, 1985, 1988), which cannot be achieved in volumes typical of protein crystals used in diffraction studies. Penetrating cryoprotectants such as glycerol and non-penetrating cryoprotectants such as large molecular weight polyethylene glycols (PEGs) can increase cooling times required for vitrification of internal and external solvent by orders of magnitude to >10 s (Angell & Choi, 1986; Sutton, 1991*a*,*b*). At concentrations typically found in protein crystals, protein itself is an excellent cryoprotectant and cooling times required to vitrify internal solvent are typically in the range 0.01–1 s (Sartor *et al.*, 1992, 1994, 1995; Sartor & Mayer, 1994; Peyrard, 2001).

Protein crystals are usually flash-cooled by inserting a crystal into a nitrogen or helium cold gas stream, or by plunging into liquid nitrogen at T = 77 K or liquid propane at T = 86 K (Teng, 1990). Experiments using a thermocouple coated with mother liquor have explored temperature evolution during flash-cooling (Teng & Moffat, 1998; Walker *et al.*, 1998) and numerical studies (Kuzay *et al.*, 2001; Nicholson *et al.*, 2001) have investigated heat transfer from crystals in high-intensity X-ray beams. Preliminary attempts to image temperature distributions during flash-cooling using infrared imaging have also been reported (Snell *et al.*, 2002). Plunge-cooling methods for cryofixation in electron microscopy and for cryopreservation have a much more extensive history of study (Ryan, 1992).

Here, we present an approximate analytical discussion of flash-cooling of protein crystals and of crystal heating by X-ray absorption. We focus on evaluating the effects of common experimental protocols and parameters on crystal cooling times, internal temperature gradients and X-ray heating. Because some variables are ill-defined and some important constants have not been measured, an exact analysis is not possible. We emphasize order-of-magnitude estimates and functional dependencies to determine the relative importance of variables under the control of the experimenter.

2. Analysis

The physics of heat transfer from solid objects in gas and liquid streams has an extensive history of experimental and theoretical study and the important results on which our analysis is based can be found in several books (Schlichting, 1979; Blevins, 1984; Rohsenow *et al.*, 1985; Kakac *et al.*, 1987; Landau & Lifshitz, 1987; Tritton, 1988; White, 1991; Bejan, 1995). The analysis that follows, although standard in most

Table 2
Thermal conductivities and heat capacities.

(*a*) Thermal conductivity of water/hexagonal ice (I_h) (Slack, 1980; Andersson & Suga, 1994; Lide, 2000), low-density amorphous (LDA) ice at 0.1 GPa (Andersson & Suga, 2002) and 30% glycerol in water (Rastorguev & Ganiev, 1966) at selected temperatures.

	κ (W m^{-1} K^{-1})		
T (K)	I_h/water	LDA ice	30% glycerol
300	0.61	n/a	0.35
273	2.1/0.56	n/a	n/a
200	3.3	n/a	n/a
100	6.5	1.1	n/a
30	20	n/a	n/a

(*b*) Heat capacity per unit mass for tetragonal lysozyme (Miyazaki *et al.*, 2000), liquid water and hexagonal ice (Lide, 2000) at selected temperatures.

	c_p (J kg^{-1} K^{-1})	
T (K)	Lysozyme	Water/I_h
300	1.8×10^3	4.2×10^3
200	1.0×10^3	1.6×10^3
100	5×10^2	9.0×10^2
30	1.6×10^2	2.9×10^2

respects, is rather involved. We have thus tried to make the discussion in §4 of results important for crystallographers as self-contained as possible. The important physical parameters used in this analysis are given in Tables 1 and 2 and are discussed in more detail in §3.

2.1. Boundary-layer approximation and the heat-transfer coefficient

We begin by considering the case of gas-stream cooling. The character of flow in a gas stream flowing from a nozzle is determined by the Reynolds number $\mathrm{Re}_f = ud/v$, where d is the diameter of the nozzle, u is the average velocity of the flow at its outlet and v is the kinematic viscosity of the gas. Using gas parameters listed in Table 1 and commercial gas-flow cooler parameters discussed in §3, Re_f is $\sim 5 \times 10^3$ for N_2 at $T = 100$ K, $\sim 5 \times 10^2$ for He at $T = 100$ K and $\sim 3 \times 10^3$ at $T = 30$ K, compared with a value of $\mathrm{Re}_{f,c} \simeq 10^3$ for the onset of instability in axisymmetric jet flow (Blevins, 1984). Although at a given temperature He flows are intrinsically more stable, samples are normally placed within ~1–2 nozzle diameters of the outlet, in the laminar core region and ahead of the turbulent shear and fully developed turbulent regions that develop downstream. Consequently, the flow near the sample for both N_2 and He is essentially laminar and the free stream flow velocity is essentially equal to the exit velocity at the nozzle.

Convective heat transfer from the surface of a crystal to a cooling fluid (gas or liquid) is determined by the character of flow (*i.e.* laminar or turbulent) in the fluid boundary layer on its surface, which depends on the Reynolds number

$$\mathrm{Re}_L = uL/v, \tag{1}$$

where L is the characteristic sample size along the flow direction. Table 3(*a*) gives estimates of Re_L, calculated using the fluid parameters in Table 1, for a typical range of crystal

Table 3
Parameters characterizing convective fluid cooling in the boundary-layer approximation for various gases and liquids and different crystal sizes, calculated using values in Tables 1 and 2 as discussed in §2.

(*a*) The Reynolds number Re_L for flow around the sample from (1). Re_L is calculated with v at 300 K for gases and at the melting point for liquids.

	Re_L		
Size L (μm)	40	200	1000
N_2 (g)	3	13	70
He (g)	0.3	1.6	8
N_2 (l)	1.7×10^2	9×10^2	4×10^3
Ethane (l)	30	1.4×10^2	7×10^2
Propane (l)	3	15	80

(*b*) The heat-transfer coefficient h from (3). h is calculated at $T = 300$ K except in the case of ethane, where $T = 273$ K is used.

	h (W m^{-2} K^{-1})		
Size L (μm)	40	200	1000
N_2 (g)	6.4×10^2	2.9×10^2	1.3×10^2
He (g)	n/a	6.1×10^2	2.7×10^2
N_2 (l)	7×10^3	3×10^3	1.4×10^3
Ethane (l)	2.2×10^4	1.0×10^4	5×10^3
Propane (l)	1.8×10^4	8×10^3	4×10^3

(*c*) The Biot number Bi from (5). Bi is calculated using the sample's thermal conductivity κ_s in the range 0.6–5 W m^{-1} K^{-1}.

	Bi		
Size L (μm)	40	200	1000
N_2 (g)	$(0.5–5) \times 10^{-2}$	0.012–0.10	0.03–0.22
He (g)	n/a	0.03–0.24	0.06–0.5
N_2 (l)	0.06–0.5	0.13–1.1	0.3–2.4
Ethane (l)	0.18–1.5	0.4–3	0.9–7
Propane (l)	0.15–1.2	0.3–3	0.7–6

sizes. All values are all well below $\sim 10^5$, where the boundary layer becomes unstable (Landau & Lifshitz, 1987; White, 1991). In the absence of the extreme shape effects that can occur for crystals with highly irregular geometries (and which are usually eliminated by surrounding mother liquor or cryoprotectant), the boundary layer in the cold flow near the sample should thus be laminar, except perhaps for the region on the downstream side of the sample where the laminar boundary layer separates.

The rate of convective heat transfer from the sample surface to the cold gas stream is described by Newton's law of cooling,

$$q'' = h(T_s - T_f), \tag{2}$$

where q'' is the rate of heat flow per unit area through the boundary layer, h is the local heat-transfer coefficient and in principle can be temperature-dependent, T_s is the temperature of the sample surface and T_f is the temperature in the cold flow outside the boundary layer. h depends on many factors including the character of the flow (laminar or turbulent) and the sample and flow geometry (Rohsenow *et al.*, 1985; Kakac *et al.*, 1987). Although h varies spatially along the surface, in most cases a simplified boundary-layer analysis with this

important quantity averaged over the entire sample surface gives a good description of the actual heat-transfer rates.

In addition to the Reynolds number characterizing the flow, heat transfer in fluids is characterized by the Prandtl number $\mathrm{Pr} = \nu/\chi$, where ν is the fluid's kinematic viscosity and χ is its thermal diffusivity. As shown in Table 1, for both N_2 and He gas Pr is close to 1, independent of the gas temperature.

From scaling analysis for fluids with $\mathrm{Pr} \simeq 1$ and with Re_L in the laminar boundary-layer regime, the average heat-transfer coefficient h over the surface of a spherical sample is approximately given by (Landau & Lifshitz, 1987; Bejan, 1995)

$$h \simeq \frac{\kappa}{\delta_t} = 0.6\frac{\kappa u^{1/2}}{(L\nu)^{1/2}}, \tag{3}$$

where δ_t is the average thickness of the laminar thermal boundary layer given by

$$\delta_t \simeq 1.7L/\mathrm{Re}_L^{1/2} = 1.7(\nu L/u)^{1/2} \tag{4}$$

and where κ is the thermal conductivity of the cooling fluid.

Experiments and numerical simulations are in agreement with (3) and (4) (Vyrubov, 1939; Liakhovski, 1940; Yuge, 1960; Whitaker, 1972; Bald, 1984; Wong *et al.*, 1986). Heat-transfer rates are larger (smaller) in the upstream (downstream) region of the sample where the boundary layer is thinner (has separated) (Renksizbulut & Yuen, 1983; Sharpe & Morrison, 1986; Wong *et al.*, 1986; Bagchi *et al.*, 2001; Balachandar & Ha, 2001). Averaging over the sample surface yields the empirical relation (3). Although primarily derived for a spherical sample, (3) is also roughly applicable to rod- or plate-like samples with their long dimension oriented parallel to the flow and with L corresponding to this dimension. Based on our analysis, we also expect that h is nearly independent of the temperature difference between sample and flow.

Table 3(*b*) gives estimates of h calculated using (3) for crystals of different size cooled from room temperature by gases at different temperatures. These are in fair agreement with values used in previous analyses: $100 < h < 250$ (Kuzay *et al.*, 2001) and $300 < h < 800$ (Nicholson *et al.*, 2001). The sevenfold difference in thermal conductivity between He and N_2 gas is partially compensated by a threefold difference in the thickness of the boundary layers, so that h differs by only a factor of $\sim$3 for both gases.

A similar approach yields estimates of h for plunge-cooling in cold liquids in the absence of boiling, also given in Table 3(*b*). From Table 1, $\mathrm{Pr} \simeq 2$ for liquid nitrogen, roughly three times that for nitrogen gas; $\mathrm{Pr} < 10$ for ethane and propane except extremely close to propane's melting point. The heat-transfer coefficient h is only weakly dependent on Pr, varying as $h \simeq \mathrm{Pr}^{0.3\ldots0.4}$ (Kramers, 1946; Ranz & Marshall, 1952*a*,*b*; Whitaker, 1972; Bald, 1984). Thus (3) should be approximately applicable for constant-velocity plunge-cooling in liquid cryogens, where u is now the plunge velocity.

For He and N_2 gases, the temperature dependencies of the kinematic viscosity ν and thermal conductivity κ cancel in (3) to make h essentially independent of temperature, so that the temperature at which ν and κ are evaluated does not matter. The situation is more complicated for liquid propane and ethane, whose viscosity ν increases steeply with decreasing temperature. In this case, the boundary layer is roughly determined by the smallest kinematic viscosity, which occurs in the warmest regions adjacent to the sample surface. Consequently, we use cooling fluid properties at the initial sample temperature $T \sim 300$ K in our estimates of h for liquids in Table 3(*b*), at sufficient pressures so that they remain liquid. The critical temperature for nitrogen $T = 126$ K is well below 300 K, so that nitrogen near the sample surface will initially be in an essentially gaseous state. To estimate the largest practical cooling rates, we calculated h at $T = 300$ K at a pressure $P = 10$ MPa, three times nitrogen's critical pressure. Because h will vary during cooling, these estimates will be less accurate than those for gases. However, as discussed later it is usually impractical to perform plunge-cooling with no boiling, so that these estimates are sufficient to guess the theoretical upper bounds on achievable cooling rates. Note that estimates of h based on boundary-layer theory are applicable only when the sample size L is much larger than the boundary layer thickness, δ_t (or $\mathrm{Re}_L >> 1$), which is true in N_2 gas at $T = 100$ K for $L >>$ 20 µm, in He gas at $T = 30$ K for $L >>$ 100 µm, in liquid N_2 for $L >> 0.2$ µm, in liquid ethane for $L >> 2$ µm and in liquid propane for $L >> 10$ µm.

2.2. Characteristic cooling times

To cool a crystal, heat must be conducted through the crystal's internal thermal conduction resistance from its interior to its surface and then through the convective thermal resistance of the gas or liquid boundary layer. The bottleneck in heat transport is determined by the ratio of the boundary-layer's heat-transport coefficient per unit area $h \simeq \kappa/\delta_t$ to the sample's thermal conductance per unit area κ_s/L, given by the Biot number (Liakhovski, 1940; Zasadzinski, 1988; Kuzay *et al.*, 2001)

$$\mathrm{Bi} = hL/\kappa_s. \tag{5}$$

Table 3(*c*) gives typical Bi values for gas-stream and liquid-plunge cooling, using values of the sample's thermal conductance discussed in §3 estimated from the data in Table 2(*a*).

For gas-stream cooling with both N_2 and He, $\mathrm{Bi} << 1$ for $L < 1$ mm over the entire experimentally relevant temperature range (accounting for uncertainties in κ_s discussed in §3). Heat transport is thus determined by the convective thermal resistance of the boundary layer. The cooling time is determined by the heat-transfer coefficient h and the sample's heat capacity $V\int\rho_s c_{ps}(T)\,\mathrm{d}T$, where V is the sample volume, ρ_s is its density and $c_{ps}(T)$ is the sample's temperature-dependent specific heat evaluated under flash-cooling conditions. Approximating the sample (crystal plus surrounding cryoprotectant) as a sphere of diameter L and using (3) to estimate h, a characteristic cooling time t_c can be obtained as

$$t_c \simeq \frac{c_{ps}\rho_s L}{6h} \approx 0.3\frac{c_{ps}\rho_s L^{3/2}\nu^{1/2}}{\kappa u^{1/2}}, \tag{6}$$

where κ is the thermal conductivity of the cooling gas. t_c corresponds roughly to a $1/e$ decay time, so the time for the crystal to reach within, say, 5% of the flow temperature is a few times longer. Estimates of t_c for a variety of experimental conditions are given in Table 4(*a*) and range from ~0.01 s for L = 40 µm crystals to a few seconds for $L \simeq 1$ mm.

For the limit of plunge-cooling in a liquid with no boiling, the situation is somewhat more complicated. For sufficiently small samples (roughly <500 µm), Bi < 1 and heat transfer is limited by the liquid boundary layer so that we can apply (6). As shown in Table 4(*a*), the characteristic cooling times for a given relative velocity u are roughly 50 times smaller than for gas-stream cooling. For sufficiently large samples (roughly >>500 µm), Bi > 1 and heat conduction through the sample itself provides the bottleneck. In this case, heat transport is determined by the heat-conductance equation and h in (6) can approximately be substituted by κ_s/L. If we further assume that $\chi_s \equiv \kappa_s/(c_{ps}\rho_s)$ is temperature-independent, the time evolution of the system is determined by the first (minimum) eigenvalue λ of the equation $\chi_s \Delta T = -\lambda T$ with the boundary condition set by the external flow temperature (Landau & Lifshitz, 1987). Assuming a spherical geometry, the characteristic plunge-cooling time for large crystals is then

$$t_c \simeq \frac{c_{ps}\rho_s L^2}{4\pi^2 \kappa_s} \approx 0.025 \frac{c_{ps}\rho_s L^2}{\kappa_s}, \qquad (7)$$

which is in fair agreement with previous work (Zasadzinski, 1988). Equating (6) and (7) yields a critical value $\mathrm{Bi} \simeq 2\pi^2/3 \approx 6$ for the transition from pure convective cooling through the boundary layer (lumped model) to bulk conduction-limited cooling (distributed model). As shown in Table 4(*a*), even for a 1 mm sample with Bi near this transition value plunge-cooling still improves cooling times by an order of magnitude.

2.3. Temperature distributions and strain during flash-cooling

The temperature distribution inside a crystal during flash-cooling can be determined by solving the heat-conduction equation for thermal diffusion. In general, this equation is non-linear since the crystal's thermal properties are temperature-dependent. However, in the case of small Bi, appropriate to gas-stream cooling and plunge-cooling of small crystals, internal spatial variations of T are small and so these properties can be assumed to be constant, even at the beginning of flash-cooling when temperature gradients and strains are largest. With the further approximations of spherical symmetry and uniform h, the temperature profile for times $t >> L^2/\chi_s$ can be determined as

$$T(r, t) - T_f = \delta T(t)[1 - (r/L)^2 \mathrm{Bi}], \qquad (8)$$

where $\delta T(t)$ is the temperature difference between the center of the sample and the cold stream and L^2/χ_s < 1 ms for a 100 µm sample in He gas. The maximum temperature gradient, which occurs at the crystal surface ($r = L/2$) at $t = 0$, is

$$|\nabla T|_{\max} = \mathrm{Bi}(T_i - T_f)/L \qquad (9)$$

Table 4
Characteristic cooling times, maximal internal temperature differences and maximum lattice strains for gas-stream and plunge-cooling of protein crystals of different sizes L calculated using parameters given in Tables 1, 2 and 3.

The sample's specific heat c_{ps} is taken at room temperature and its density ρ_s was assumed to be 1.2 g cm^{-3}. The sample's thermal conductivity κ_s is assumed to lie in the range 0.6–5.0 W m^{-1} K^{-1}.

(*a*) Characteristic cooling time t_c from (6) and (7).

	Cooling time t_c (s)		
Size L (µm)	40	200	1000
Gas cooling in			
N_2 at 100 K	0.022	0.24	2.7
He at 100 K	n/a	0.10	1.1
He at 30 K	n/a	0.10	1.1
Plunge in			
N_2 at 63 K	2.0×10^{-3}	2.3×10^{-2}	0.3
Ethane at 90 K	7×10^{-4}	8×10^{-3}	9×10^{-2}
Propane at 86 K	1.0×10^{-3}	1.1×10^{-2}	0.12

(*b*) Maximum internal temperature difference ΔT from (10).

	ΔT (K)		
Size L (µm)	40	200	1000
Gas cooling in			
N_2 at 100 K	0.27–2.2	0.6–5	1.3–11
He at 100 K	n/a	1.4–12	3.2–27
He at 30 K	n/a	1.9–16	4–40
Plunge in			
N_2 at 63 K	3–26	7–60	16–130
Ethane at 90 K	7–60	16–130	40–200
Propane at 86 K	5–40	11–100	26–200

(*c*) Maximum lattice strain from (14).

	Strain (%)		
Size L (µm)	40	200	1000
Gas cooling in			
N_2 at 100 K	$(1.1–9) \times 10^{-3}$	$(0.24–2.0) \times 10^{-2}$	$(0.5–4) \times 10^{-2}$
He at 100 K	n/a	$(0.6–5) \times 10^{-2}$	0.013–0.11
He at 30 K	n/a	$(0.8–7) \times 10^{-2}$	0.017–0.14
Plunge in			
N_2 at 63 K	0.013–0.10	0.03–0.23	0.06–0.5
Ethane at 90 K	0.03–0.25	0.07–0.6	0.15–0.7
Propane at 86 K	0.020–0.17	0.05–0.4	0.10–0.7

and the maximum temperature difference between the crystal's surface and center is

$$\Delta T \equiv T(0, 0) - T(L/2, 0) \simeq \mathrm{Bi}(T_i - T_f)/4. \qquad (10)$$

The time-dependent prefactor $\delta T(t)$ in (8) satisfies $c_{ps}(T)\,\mathrm{d}(\delta T)/\mathrm{d}t = h(\delta T)$. Since the sample's heat capacity varies approximately linearly with temperature $[\delta T(t) - \delta T(0)]/\delta T(0) = -t/t_c$ as long as $\delta T(t) > T_f$, where t_c is given by (6) with c_{ps} taken at T_i and h is assumed to be temperature independent, as we expect.

Table 4(*b*) gives the maximum internal temperature differences ΔT calculated using (10) for gas-stream and liquid plunge-cooling without boiling under a range of experimental conditions. As expected, the maximum internal temperature differences for gas-stream cooling are small: a few kelvin or

less in ordinary-size crystals and ~5–15 K even in 1 mm crystals. On the other hand, liquid-plunge cooling without boiling may produce extremely large temperature gradients: in a 1 mm crystal the temperature at the crystal surface may approach its final temperature before the temperature at the center has dropped appreciably. The approximation of temperature-independent sample properties that leads to (6) and (8)–(10) break down for such large temperature differences and therefore these estimates for large crystals are more qualitative.

The temperature distribution from (8) can in principle be used together with the temperature-dependent protein unit-cell parameters to calculate the strain within the crystal using the standard theory of elasticity (Landau & Lifshitz, 1986). However, protein crystals are composite materials (Juers & Matthews, 2001; Kriminski *et al.*, 2002) and as temperature decreases the internal solute may expand while the protein lattice shrinks. The interactions between proteins are short-range and can be strongly isotropic (Lomakin *et al.*, 1999) and the important bonding interactions may involve only a small fraction of each molecule's surface (Wukovitz & Yeates, 1995). Together with the structural changes that macromolecules often undergo during cooling, these properties may complicate analysis of the crystal's elastic and plastic response, especially when temperature variations are large. However, Brillouin scattering measurements of the elastic modulus tensor of lysozyme (Speziale *et al.*, 2003) suggest that protein crystals behave much like ordinary small-molecule crystals, at least at room temperature, and there is no other experimental evidence at present suggesting anomalous behavior. In any case, our results are likely to remain qualitatively and semi-quantitatively correct.

With the simplifying assumptions of spherical symmetry and small strains (Landau & Lifshitz, 1986), the displacement vector **w** is purely radial and satisfies

$$\frac{\mathrm{d}}{\mathrm{d}r}(\operatorname{div}\mathbf{w}) = \alpha_L \frac{1+\sigma}{1-\sigma}\frac{\mathrm{d}T}{\mathrm{d}r}, \qquad (11)$$

where σ is the adiabatic Poisson ratio, α_L is the linear coefficient of thermal expansion and **w** is defined so that it is zero when the entire sample is at the temperature of its surface. (11) can be solved with the boundary conditions that at $r = 0$ the displacement must be finite and that at $r = L/2$ (the sample surface) the radial component of the stress $\sigma_{rr} = E[\mathrm{d}w_r/\mathrm{d}r + \sigma \operatorname{div}\mathbf{w}/(1 - 2\sigma)]/(1 + \sigma)$, where E is the Young's modulus, must vanish.

The strain – equal to the local deviation of lattice spacing from its relaxed value at the local temperature – is obtained by subtracting the equilibrium lattice-spacing change appropriate to the local temperature, given by $\alpha_L \mathrm{Bi}\delta T[r^2 - (L/2)^2]/L^2$, from $\mathrm{d}w/\mathrm{d}r$ for the strain's radial component and from w/r for its tangential component. The resulting strains are

$$\text{radial strain} = \frac{\alpha_L \mathrm{Bi}\delta T}{5(1-\sigma)}\left[2(1-4\sigma)\frac{r^2}{L^2} - \frac{1-2\sigma}{2}\right] \qquad (12)$$

and

$$\text{tangential strain} = \frac{\alpha_L \mathrm{Bi}\delta T}{5(1-\sigma)}\left[2(2-3\sigma)\frac{r^2}{L^2} - \frac{1-2\sigma}{2}\right]. \qquad (13)$$

The outermost shell of the sample cools faster and wants to contract towards the equilibrium lattice spacing corresponding to its local temperature, but it is prevented from doing so by the force exerted on the shell by the warmer region inside which has contracted less. As a result, the sample's outer shell is under tension (tangential strain > 0) and its inner part is under compression; the radial strains are compressive (<0) throughout the sample and largest at the surface. The maximum positive tangential strain (at the sample surface) is given by

$$\text{maximum positive strain} \simeq \alpha_L \mathrm{Bi}\delta T/10 \qquad (14)$$

and the maximum negative radial strain has the same magnitude. Protein crystals are more easily damaged under tension (positive strain) than under compression (negative strain) (Morozov & Morozova, 1993) so that the maximum positive tangential strain (14) determines the onset of plastic failure.

Table 4(*c*) gives estimates of the maximum strain under a range of gas-stream and plunge-cooling conditions with parameters as discussed in §3. For gas-stream cooling the maximum strains are generally small compared with estimated yield strains of ~2–3% (Gorelov & Morozov, 1987; Morozov & Morozova, 1993) and with lattice-constant spreads observed in crystals that diffract poorly after flash-cooling of ~1–2% (Kriminski *et al.*, 2002). The only exception is for helium cooling of large (≥1 mm) crystals that have larger expansion coefficients, where strains may be large enough to be problematic, especially given uncertainties in yield strains. Crystals with high defect densities (cracks, inclusions, grain boundaries) before flash-cooling may have smaller yield strains and thus be more susceptible to cooling damage.

On the other hand, maximum strains in crystals that are plunge-cooled without boiling are large (up to ~1%) even in 40 µm crystals. As is seen from Table 1 of Juers & Matthews (2001), the coefficient of linear thermal expansion α_L varies between protein crystals by nearly two orders of magnitude, implying a corresponding variation in optimal cooling rate.

2.4. Heating by X-ray absorption

Heating by X-ray absorption has recently been analyzed by Kuzay *et al.* (2001). Here, we present improved and extended analytical estimates and a possible strategy for reducing heating.

We assume a spherical sample of diameter L small compared with the X-ray absorption length L_{abs}, so that absorption is roughly uniform throughout the crystal volume. The maximum (steady-state) temperature increase arising from absorption can be calculated by balancing the convective heat-transfer rate through the gas boundary layer with the absorbed X-ray power $P_{\mathrm{abs}} \simeq IV/L_{\mathrm{abs}}$, where I is the X-ray energy flux in W m^{-2} (equal to the photon flux × $\hbar\omega$), V is the sample volume and I/L_{abs} is the absorbed power per unit volume. The steady-state increase of the sample's surface temperature T_s relative to T_f of the bulk gas stream, obtained

Table 5
Effects of X-ray absorption on a sample in cold He and N_2 gas streams, assuming an incident flux of 5×10^{12} photons s^{-1} mm^{-2} at 13 keV and an absorption length $L_{abs} \simeq 3.8$ mm corresponding to a metal-free crystal with 40%(*w*/*w*) of water.

The calculations assume a sample thermal conductivity κ_s in the range 0.6–5 W m^{-1} K^{-1} and a sample density ρ_s of 1.2 g cm^{-3}. The sample's specific heat c_{ps} is taken from Table 2. For a SeMet derivative at the Se *K* absorption edge used in MAD phasing [where $L_{abs} \simeq 2.3$ mm for 40%(*w*/*w*) water], the calculated temperature rise is 1.6 times larger.

(*a*) Estimated crystal heating as given by (15).

	ΔT (K)		
L (μm)	40	200	1000
N_2 (g)	0.026	0.31	3.6
He (g)	n/a	0.13	1.5

(*b*) Equilibration time t_e from (17).

	t_e (s)		
L (μm)	40	200	1000
N_2 (g), 100 K	6×10^{-3}	7×10^{-2}	0.8
He (g), 100 K	n/a	2.8×10^{-2}	0.3
He (g), 30 K	n/a	9×10^{-3}	0.10

(*c*) Estimated maximum internal temperature variations between sample center and surface from (16).

	Internal ΔT (K)		
L (μm)	40	200	1000
N_2 (g) and He (g)	(4–31) $\times 10^{-5}$	(1.0–8) $\times 10^{-3}$	(2–20) $\times 10^{-2}$

by assuming a constant h given by (3), integrating (2) over the surface of the sphere and equating the result with P_{abs}, is

$$T_s - T_f \simeq \frac{L}{6h}\frac{I}{L_{abs}} \approx 0.3\frac{L^{3/2}\nu^{1/2}}{\kappa u^{1/2}}\frac{I}{L_{abs}} \qquad (15)$$

and is inversely proportional to the X-ray absorption length. The temperature profile within the spherical sample is given by

$$T(r) = T_s + \frac{I}{L_{abs}}\frac{(L/2)^2}{6\kappa_s}\left[1 - \left(\frac{r}{L/2}\right)^2\right]. \qquad (16)$$

The ratio of the internal temperature difference $T(r = 0) - T_s$ to the difference $T_s - T_f$ is Bi/4. Consequently, temperature variations within the sample are small compared with the average temperature rise $\sim T_s - T_f$ except in very large samples (for which our assumption $L << L_{abs}$ may also break down).

The equilibration time required after the beam is turned on is roughly

$$t_e \simeq c_{ps}\rho_s(T_s - T_f)L_{abs}/I, \qquad (17)$$

which is similar to (6) but with the sample's specific heat now evaluated at the gas-stream temperature. For exposure times that are short compared with this equilibration time, *e.g.* as may occur during time-resolved Laue diffraction experiments (Moffat, 1989; Nave, 1995), adiabatic heating can be assumed and the crystal temperature increases linearly with exposure time Δt: $\Delta T = I\Delta t/(c_{ps}\rho_s L_{abs})$.

As shown in Table 5, using a flux typical of macromolecular crystallography beamlines at third-generation synchrotron sources, a typical absorption length for a metal-free protein crystal at an X-ray energy of 13 keV and a size $L = 200$ μm gives a temperature rise $T_s - T_f$ in a nitrogen cold gas stream at $T = 100$ K of ∼0.3 K. The corresponding equilibration time is ∼0.1 s and the internal temperature difference $T_s - T_c$ is only $(1.0 - 8) \times 10^{-3}$ K. The results in Table 5 are more reliable than those of earlier work based on a simplified geometry and a different estimate for h (Kuzay *et al.*, 2001).

3. Materials properties and parameter estimates

3.1. Characteristics of gas streams and liquid cryogens

Table 1 gives established values for the thermal conductivity, kinematic viscosity, thermal diffusivity and Prandtl number of nitrogen and helium gases and of liquid nitrogen, propane and ethane at selected temperatures.

From the manufacturers' literature, the speed u of gas-stream flows in current commercial gas-stream coolers is typically 1–2 m s^{-1}. Typical liquid plunge-cooling velocities are similar and so for both gas-stream and plunge-cooling we use a value $u = 1$ m s^{-1} for the flow velocity in calculating the convective heat-transfer coefficient h. We assume a gas-stream flow diameter $d \simeq 1$ cm.

3.2. Characteristics of the sample

Table 2(*b*) gives specific heats at selected temperatures of tetragonal lysozyme crystals (Miyazaki *et al.*, 2000), water and hexagonal ice (Lide, 2000). Excluding the latent heat associated with formation of internal hexagonal ice during slow cooling, the specific heat of tetragonal lysozyme varies approximately linearly with temperature between room temperature and $T = 100$ K, similar to polyamino acids (Roles & Wunderlich, 1991). We assume a sample specific heat $c_{ps}(T) = 6.0$ J kg^{-1} K^{-2} $\times$ T and a density $\rho_s = 1.2 \times 10^3$ kg m^{-3} (Steinrauf, 1959).

The thermal conductivity of protein crystals has not been measured. Most organic liquids have thermal conductivities in the range 0.1–0.3 W m^{-1} K^{-1} at $T = 250$ K and that are several times larger at $T \simeq 100$ K (Lide, 2000). Thermal conductivities for hexagonal ice, given in Table 2(*a*), range from 0.56 W m^{-1} K^{-1} at $T = 273$ K to 5.7 W m^{-1} K^{-1} at $T = 110$ K (Lide, 2000). Room-temperature thermal conductivities of protein-rich [∼20–25%(*w*/*v*)] foods such as fish and beef are in the range 0.3–0.6 W m^{-1} K^{-1} (Krokida *et al.*, 2002). Accounting for the 30–60% water content of typical crystals we assume κ_s for protein crystals varies from ∼0.6 to ∼5.0 W m^{-1} K^{-1} between room temperature and $T = 100$ K. The Biot number Bi, the internal sample temperature difference ΔT and the strain are inversely proportional to κ_s and thus have uncertainties related to κ_s of at least a factor of 2.

Thermal expansion data for a variety of protein crystals derived from their unit-cell parameters are nicely summarized

in Table 1 of Juers & Matthews (2001). The values of the linear expansion coefficient quoted range from 10^{-6} to $1.3 \times 10^{-4}\,K^{-1}$, with a mean of $8 \times 10^{-5}\,K^{-1}$. As discussed in Kriminski *et al.* (2002), because of differential expansion of solvent and protein lattice these values do not necessarily match the expansion behavior of the crystal as whole, but they should be close for crystals that have been properly cryoprotected. Similar values of $3–4 \times 10^{-5}\,K^{-1}$ were obtained for a variety of amorphous protein films by direct measurements (Morozov & Gevorkian, 1985). We assume a value $\alpha_L = 1 \times 10^{-4}\,K^{-1}$, comparable to the values reported for tetragonal lysozyme [$8 \times 10^{-5}\,K^{-1}$ by Young *et al.* (1994) and $1.2 \times 10^{-4}\,K^{-1}$ at $T < 250$ K by Kurinov & Harrison (1995)]. The Poisson ratio σ has not been measured and so we assume a value $\sigma = 0.33$ typical of polymers and polycrystalline ice (Gammon *et al.*, 1983).

We assume a value of the yield strain for protein samples of 2–3%, as has been determined in room-temperature measurements (Gorelov & Morozov, 1987). Because of the composite nature of protein crystals, it is difficult to predict the temperature-dependence of the yield strain; based on measurements on ice (Jones & Glen, 1969), low-temperature yield strains probably show significant crystal-to-crystal variations. In addition, yield strains often depend strongly on strain rate (Higashi, 1969). However, the Young's modulus of protein crystals increases by a factor of 10 on cooling to $T = 100$ K (Morozov & Gevorkian, 1985) and based on the behavior of ice (Xu *et al.*, 2003) we expect the yield stress to increase by a similar factor. Consequently, as in polymers (Brooks *et al.*, 1999) we expect that the yield strain is approximately temperature independent.

3.3. X-ray absorption parameters

X-ray absorption lengths L_{abs} at $E = 13$ keV calculated for protein crystals with 40% solvent content are ~3.8 mm for metal-free protein crystals and ~2.3 mm for both heavy-atom derivatives and for SeMet derivatives at the Se absorption edge, consistent with previous estimates at 8 keV (Henderson, 1990). The flux at a third-generation synchrotron protein crystallography beamline (*e.g.* the 14-ID wiggler station at the Advanced Photon Source or APS) is about 5×10^{12} photons $s^{-1}mm^{-2}$ for a 0.1% bandwidth. With a photon energy of 13 keV, this corresponds to an intensity of $\sim 10^4$ W m^{-2}.

4. Results and implications for cryocrystallography

The analysis in §2 of flash-cooling in cold gas streams and by plunge-cooling in cold liquids used the laminar boundary layer approximation to determine the rate of convective heat transfer from the crystal. Our simplified analysis based largely on scaling arguments is in good agreement with the results of more rigorous calculations of related heat-transfer problems and with simulations and experiments for more realistic geometries. In this section, we summarize the important results of our analysis and discuss their implications for cryocrystallography. Fig. 1 summarizes our results for characteristic cooling times *versus* crystal size.

4.1. Flash-cooling in cold gas streams

Heat is conducted from the crystal interior to its surface and is then convected away from its surface through the gas boundary layer to the bulk flowing gas. Heat transfer through the boundary layer is the rate-limiting step except for extremely large (>>1 mm) crystals.

4.1.1. Characteristic cooling times. Based on parameter estimates in Table 1, for a 200 μm protein crystal the characteristic time t_c to cool from room temperature to below T_g, the glass-transition temperature of water, is of the order of 0.2 s. Table 4(*a*) gives estimates of characteristic cooling times with different gases and liquids and for different crystal sizes. The results are consistent with previous experiments using small liquid-coated thermocouples, which gave cooling times in nitrogen-gas streams of ~2 s for a ~700 μm sample (Walker *et al.*, 1998) and 1–2 s for a ~900 μm sample (Teng & Moffat, 1998).

4.1.2. Temperature gradients and internal stresses. Equilibration times within the crystal are much shorter than between the crystal and flowing gas, except perhaps in very large (>1 mm) helium-cooled crystals. As shown in Table 4(*b*), temperature differences between the center and surface of the crystal ΔT are thus extremely small (less than ~30 K even in 1 mm samples flash-cooled in a He stream) and thermally induced internal strains are likely to be too small (<0.1%) to cause significant crystal damage, except perhaps in crystals with pre-existing cracks or other damage. The degradation of diffraction properties that often accompanies flash-cooling is then primarily a consequence of homogeneous processes,

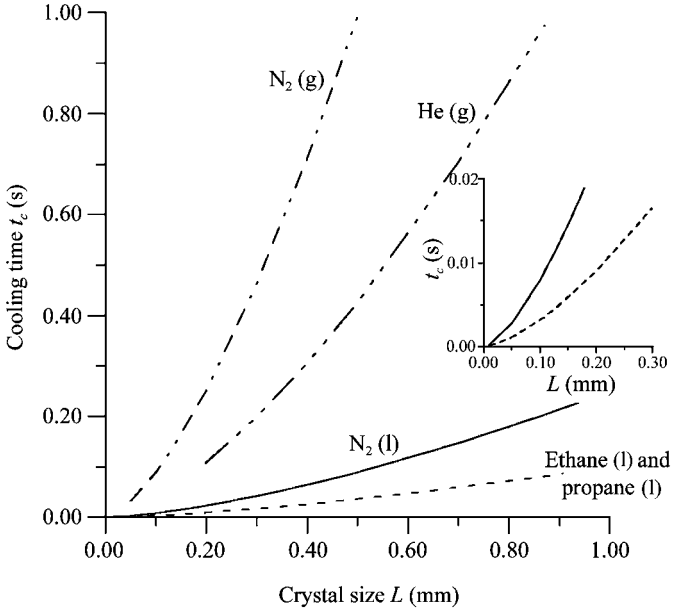

Figure 1
Sample cooling time t_c for different flash-cooling methods (gas stream *versus* liquid plunge without boiling) and cooling fluids *versus* sample size L. The inset is an expanded view of the liquid plunge-cooling times for smaller sample sizes. Axes of the inset are the same as in the main figure.

consistent with recent X-ray topography studies (Kriminski *et al.*, 2002). This assumes that the crystal's thermal expansion is linear (Kurinov & Harrison, 1995). However, if thermal expansion is step-like, for example owing to a structural transformation of the protein, protein lattice or solvent, even small internal temperature gradients may cause significant lattice mismatch and damage (Dobrianov *et al.*, 2001; Kriminski *et al.*, 2002).

4.1.3. Effect of crystal size and shape. For a near-spherical or cubic-shaped crystal of linear size L, the characteristic cooling time $t_c \propto L^{3/2}$ and the maximum temperature difference between the interior and surface of the crystal $\Delta T \propto L^{1/2}$. As Table 4(*a*) shows, the former relation translates into a factor of ~125 difference in cooling times between crystals with L = 40 µm and L = 1 mm. For crystals with plate-like shapes $t_c \propto L^{1/2}\theta$ and $\Delta T \propto \theta/L^{1/2}$, where θ is the sample thickness.

4.1.4. Effect of surrounding mother liquor or cryoprotectant. For small (<100 µm) crystals mounted in nylon or metal loops (Teng, 1990), the volume of surrounding mother liquor or cryoprotectant can be comparable to or larger than the crystal volume. Because this liquid has similar thermal properties to the crystal (whose largest component by volume is often solvent), the effective sample size L in cooling calculations is determined by the total size of the crystal plus liquid, increasing required cooling times. For irregularly shaped crystals, surrounding mother liquor/cryoprotectant also rounds out the effective shape of the frozen composite sample, simplifying gas-flow patterns and temperature fields around its surface.

4.1.5. Effect of gas temperature. The cooling rate for convective heat transfer is linearly proportional to the difference between the initial crystal temperature T_i and the bulk gas temperature T_f: $q'' \propto T_i - T_f$. For helium gas at T = 100 and 30 K, the cooling rate ratio is ~1.4.

4.1.6. Effect of gas type. The cooling time varies with the kinematic viscosity ν and thermal conductivity κ of the gas as $t_c \propto \nu^{1/2}/\kappa$. Although helium has a much larger thermal conductivity, its kinematic viscosity is also larger. Switching from nitrogen gas to helium gas at fixed gas-stream temperature and flow speed increases the characteristic cooling rate by a factor of ~2. Switching from nitrogen at T = 100 K to helium at T = 30 increases the cooling rate by a factor of ~3.

4.1.7. Effect of gas velocity. The cooling time varies with gas velocity u as $t_c \propto u^{-1/2}$; therefore doubling the gas velocity decreases the cooling time by a factor of 1.4 or ~30%. Increases in gas velocity may be limited by the onset of turbulence and by crystal movements caused by the fluctuating drag force on the crystal and its mount.

4.1.8. Effect of crystal solvent content. In the absence of penetrating cryoprotectants, increasing the crystal solvent content increases the minimum cooling rates required to achieve amorphous solvent, with a rapid increase occurring beyond ~40%(*w*/*w*) (Sartor *et al.*, 1995). This corresponds to completion of the second hydration shell (Yang & Rupley, 1979), where the cryoprotective effects of hydrogen bonding between water and protein become exhausted. As solvent content is varied from 20 to 90%, the required cooling rates increase by several orders of magnitude. For a given solvent content, the presence of large solvent channels within the crystal structure may also dramatically increase the required cooling rates (Weik *et al.*, 2001). These large cooling rates in solvent-rich crystals can in turn be dramatically reduced into the experimentally accessible range using penetrating cryoprotectants such as glycerol.

A much smaller effect arises from the large enthalpy that must be removed from water when it is flash-cooled into amorphous ice (which includes a significant fraction of the latent heat of the water–hexagonal ice transition). The required enthalpy for 80% solvent-content crystals is roughly 25% larger than for those with 40% solvent content, producing a comparable ratio of cooling times.

4.2. Flash-cooling in cold liquids

The shortest cooling times can be achieved by plunging crystals at a velocity u into a liquid cryogen and by choosing conditions so that the liquid near the crystal does not boil and produce an insulating vapor layer. Boiling can be eliminated by using liquid cryogens that have a large spread between their melting and boiling temperatures (such as propane and ethane), by applying pressure to raise the boiling temperature and increase this spread and by using these cryogens near their melting point and by using very small crystals.

Largely for reasons of experimental convenience, the plunge-cooling protocols used by crystallographers (*e.g.* with liquid nitrogen at T = 77 K) usually produce significant boiling, so that cooling times are improved by only a factor of ~2 over those achieved in gas streams (Teng & Moffat, 1998; Walker *et al.*, 1998). Analyzing heat transfer in the presence of boiling is extremely complex and is well beyond the scope of the present work; experiments such as those cited above are likely to remain the easiest way to evaluate cooling times with boiling. But how much improvement is possible in principle in the absence of boiling?

4.2.1. Characteristic cooling times. As shown in Table 4(*a*) and consistent with previous estimates (Bald, 1984), plunge-cooling without boiling should reduce cooling times by more than an order of magnitude compared with gas cooling.

4.2.2. Temperature gradients and internal stresses. Because heat transfer using liquids is much more efficient than with gases, the bottleneck to heat transfer is provided by the liquid-boundary layer only for crystals of size L roughly <500 µm. In larger crystals, heat conduction through the crystal itself becomes important and temperature gradients become appreciable. A rough estimate given in Table 4(*b*) suggests internal temperature differences of ~200 K in 1 mm crystals, which will produce strains of ~1%. This is comparable with measured yield strains in protein crystals (Morozov & Morozova, 1993) and to strains measured in protein crystals that have been heavily disordered by flash-cooling (Kriminski *et al.*, 2002).

The more rapid cooling rates provided by plunge-cooling without boiling are most important for larger crystals (>500 μm) and for crystals with large amounts of surrounding solvent (which crystallizes much more easily than internal solvent). They are also important for high solvent-content crystals, whose gas-stream cooling rates are often insufficient to prevent internal water crystallization in the absence of cryoprotectants. This analysis suggests that the advantages of liquid plunge-cooling without boiling for larger crystals (which cool more slowly) and high solvent-content crystals (which are more mechanically fragile) – reduced crystal damage owing to solvent expansion and crystallization and owing to protein conformation changes – may be offset by increased crystal damage owing to larger thermal stresses and lattice strains. The plunge-cooling methods normally used by crystallographers, which can involve significant boiling and provide more modest increases in cooling rates, may thus provide a reasonable compromise between larger cooling rates and larger thermomechanical stresses.

4.2.3. Effect of crystal size. For smaller crystals in which cooling rates are limited by convection, $t_c \propto L^{3/2}$ as for flash-cooling in gases. However, for larger crystals (roughly >500 μm) where internal conduction is important, $t_c \propto L^2$ and the size dependence becomes even stronger.

4.2.4. Effect of liquid temperature, type and plunge velocity. For small crystals, the dependencies on liquid temperature, type and relative (in this case, plunge) velocity are the same as for gas-stream cooling. Ethane and propane are more effective coolants than nitrogen because of their higher critical temperature and large spread between melting and boiling temperatures. For large crystals, heat conduction within the crystal dominates and the dependence on liquid properties and plunge velocity disappears.

4.3. Optimizing flash-cooling

When optimizing flash-cooling protocols, one tries to achieve a cooling rate sufficient to produce solvent vitrification by increasing the physical cooling rate and/or decreasing the cooling rate required to achieve vitrification. Based on the preceding discussion, we can order the important experimental factors in terms of their relative effects on solvent vitrification as follows.

(*a*) Factors with large effects.

(i) Crystal solvent content.

(ii) Penetrating cryoprotectant concentration.

(iii) Crystal size.

(iv) Amount and cryoprotectant concentration of excess surrounding liquid.

(v) Liquid plunge-cooling *versus* gas-stream cooling.

(*b*) Factors with modest effects.

(i) Liquid/gas type and temperature.

(ii) Gas flow/plunge velocity.

Large improvements in cooling times should be routinely obtained by using the small crystal sizes (∼50 μm) made possible by high-flux beamlines, minimizing solvent volume surrounding the crystal and plunge-cooling in liquid propane or ethane at ambient pressure just above their melting points. Until a convenient high-throughput apparatus is developed, the full benefits of high-pressure plunge-cooling with no boiling for small crystals (for which thermal gradients and stresses are small) are unlikely to be routinely achieved.

Reducing crystal solvent contents may be more challenging. Proteins can usually be grown in different crystal forms with different solvent contents and solvent channel sizes, but identifying a low solvent-content form that diffracts well can often be difficult. Dehydration prior to flash-cooling may provide a more routine approach. While strong dehydration may completely destroy diffraction quality, weak dehydration to remove bulk-like water (keeping the first and second hydration layers intact) may improve flash-cooling properties with minimal effect on molecular structure and possibly beneficial effect on resolution (Kiefersauer *et al.*, 2000; Dobrianov *et al.*, 2001).

Optimizing cryoprotection is a standard part of cryocrystallographic practice and is described in many review articles. One crucial but often overlooked point is that the freezing behaviors and thus the required cryoprotection protocols for internal and external solvent are very different. Kriminski *et al.* (2002) give a discussion of the physics of cryodamage and cryoprotection that may eventually lead to improved protocols.

4.4. Crystal heating by X-ray absorption

Protein crystal heating in cold gas streams by X-ray absorption becomes more important as the flux and brilliance of X-ray sources increases. Heating can damage crystals by allowing conformation changes (Tilton *et al.*, 1992), protein lattice relaxation, solvent diffusion and crystallization, as well as diffusion and reaction of absorption-induced free radicals.

The factors listed above that control flash-cooling times in gas streams also determine absorption-induced temperature rises. For a crystal with $L < 1$ mm in a cold gas stream and uniformly illuminated with X-rays over its entire volume, the temperature rise owing to X-ray absorption is $\Delta T \propto L^{3/2}\nu^{1/2}/\kappa u^{1/2}$. This shows the same dependencies on crystal size L, gas type and flow velocity u as does the characteristic time for flash-cooling. Crystal size is again the largest variable factor and using helium instead of nitrogen as the cooling gas can reduce heating by a factor of ∼3. Estimates in Table 5(*a*) using X-ray fluxes at third-generation wiggler beamlines, *e.g.* 14-ID at the Advanced Photon Source, yield temperature changes for typical protein crystals of only a few kelvin.

Absorption can increase by ∼50% in crystals containing metals or heavy atoms or when data is collected near absorption edges as in multiple-wavelength anomalous diffraction (MAD) phasing (Hendrickson, 1991), producing a proportionate increase in temperature. Absorption decreases and the absorption length increases with X-ray energy. For example, if the energy is increased from 8 to 13 keV, the absorption length will be four times larger and the temperature rise about 2.5 times smaller. In the usual range of X-ray

energies used in crystallography, absorption occurs primarily *via* the photoelectric effect, so that $L_{\rm abs} \simeq E^3$ and $\Delta T \simeq E^{-2}$.

Heating effects can be reduced by cooling with helium gas at a temperature T = 30 K. This improves h and is likely to increase the sample's thermal conductivity κ_s, the latter being especially important when only a small part of the crystal volume is illuminated, as will be discussed below. It also gives more 'headroom' between the base temperature and water's glass transition $T_g \simeq 140$ K, at which substantial internal relaxation, diffusion and recrystallization typically begins (Miyazaki *et al.*, 2000; Weik *et al.*, 2001), allowing larger temperature rises to be tolerated. Assuming a maximum tolerable temperature of T = 120 K, an X-ray energy of 13 keV, an absorption length $L_{\rm abs} \simeq 2.3$ mm and a sample size L = 200 µm gives a maximum allowed flux of $\sim 3 \times 10^{15}$ photons s^{-1} mm^{-2} with a He gas stream at 30 K and $\sim 3 \times 10^{14}$ photons s^{-1} mm^{-2} with a N_2 gas stream at 100 K. Both values can be exceeded, *e.g.* in undulator mode on beamline 14-ID at the APS.

For a given illuminated area (X-ray spot size), heating can be reduced by using larger crystals and especially by using plate-like crystals. Heat transfer occurs much more easily through the crystal than through the gas boundary layer. The region of a crystal outside of the illuminated volume can thus act as a heat sink or 'fin', conducting heat to a crystal surface having a larger area than the illuminated volume for convective heat transfer to the gas. For a beam size L_b, a spherical or cubic crystal of size $L > L_b$ has a surface area $(L/L_b)^2$ larger, a heat-transfer coefficient $(L_b/L)^{1/2}$ smaller and an illuminated volume L/L_b larger than a crystal of size L_b. The temperature rise owing to absorption is then smaller by a factor $(L_b/L)^{1/2}$. For a plate-like crystal of plate thickness L_b and width L oriented with the thickness roughly along the incident beam and with the gas flow perpendicular to the beam, the illuminated volume is the same as for a crystal of size L_b, the surface area is larger by a factor $\sim(1/3)(L/L_b)^2$ and the temperature jump is smaller by a factor $\sim 3(L_b/L)^{3/2}$. For example, with L = 300 µm and L_b = 30 µm, a plate-like crystal will have a factor of $\sim$30 smaller temperature rise than a cubic crystal of size $L = L_b$. The heat-sinking effect is cut off at large crystal sizes $L^2 \simeq (\kappa_s/h)L_b$, when heat transfer is no longer limited by external convection. Note that only the illuminated portion of the crystal need be highly ordered; the portion outside the illuminated volume can be cracked, twinned or damaged and still serve as an effective heat sink. Heat sinking and smaller temperature increases could also be achieved by encasing a crystal of size L_b in a highly thermally conducting material (Nicholson *et al.*, 2001). However, finding such a non-crystalline material that does not absorb X-rays or contribute significantly to background scatter may be challenging.

5. Conclusion

We have presented an approximate analysis of heat transfer from protein crystals and have applied it to the problems of flash-cooling and X-ray heating. Based on this analysis, we have extracted the important functional dependencies of cooling times, temperature rises and other quantities on the parameters under control of the experimenter. We have also compiled a list of experimental values of important physical parameters and made estimates of others to obtain order-of-magnitude numerical results. Together, we hope these results will provide some guidance in designing experimental protocols for cryocrystallography. A more quantitative analysis awaits measurements of the temperature-dependent thermal conductivity and other physical properties of protein crystals.

We which to thank V. Berezhnov, C. L. Henley, E. Kalinin and J. P. Sethna for fruitful discussions. This work was supported by the NIH (R01 GM65981-01) and by NASA (NAG8-1831).

References

Andersson, O. & Suga, H. (1994). *Phys. Rev. B*, **50**, 6583–6588.
Andersson, O. & Suga, H. (2002). *Phys. Rev. B*, **65**, 140201.
Angell, C. A. & Choi, Y. (1986). *J. Microsc.* **141**, 251–261.
Bagchi, P., Ha, M. Y. & Balachandar, S. (2001). *J. Fluids Eng. Trans. ASME*, **123**, 347–358.
Balachandar, S. & Ha, M. Y. (2001). *Phys. Fluids*, **13**, 3714–3728.
Bald, W. B. (1984). *J. Microsc.* **134**, 261–270.
Barkalov, I. M., Bolshakov, A. I., Goldanskii, V. I. & Krupyanskii, Y. F. (1993). *Chem. Phys. Lett.* **208**, 1–4.
Bejan, A. (1995). *Convection Heat Transfer.* New York: John Wiley.
Blevins, R. D. (1984). *Applied Fluid Dynamics Handbook*. New York: Van Nostrand Reinhold Co.
Brooks, N. W. J., Duckett, R. A. & Ward, I. M. (1999). *Polymer*, **40**, 7367–7372.
Bruggeller, P. & Mayer, E. (1980). *Nature (London)*, **288**, 569–571.
Chayen, N. E., Boggon, T. J., Cassetta, A., Deacon, A., Gleichmann, T., Habash, J., Harrop, S. J., Helliwell, J. R., Nieh, Y.-P., Peterson, M. R., Raftery, J., Snell, E. H., Hädener, A., Niemann, A. C., Siddons, D. P., Stojanoff, V., Thompson, A. W., Ursby, T. & Wulff, M. (1996). *Q. Rev. Biophys.* **29**, 227–278.
Dobrianov, I., Kriminski, S., Caylor, C. L., Lemay, S. G., Kimmer, C., Kisselev, A., Finkelstein, K. D. & Thorne, R. E. (2001). *Acta Cryst.* D**57**, 61–68.
Gallian, R. W. & Yaws, C. L. (1992). *Physical Properties of Hydrocarbons.* Houston: Gulf Publication Co.
Gammon, P. H., Klefte, H. & Clouter, M. J. (1983). *J. Phys. Chem.* **87**, 4025–4029.
Garman, E. (1999). *Acta Cryst.* D**55**, 1641–1653.
Garman, E. F. & Schneider, T. R. (1997). *J. Appl. Cryst.* **30**, 211–237.
Gorelov, A. V. & Morozov, V. N. (1987). *Biophys. Chem.* **28**, 199–205.
Henderson, R. (1990). *Proc. R. Soc. London Ser. B*, **241**, 6–8.
Hendrickson, W. A. (1991). *Science*, **254**, 51–58.
Higashi, A. (1969). *Mechanical Properties of Ice Single Crystals*. Munich, Germany: Plenum Press.
Hope, H. (1990). *Annu. Rev. Biophys. Biophys. Chem.* **19**, 107–126.
Jones, S. J. & Glen, J. W. (1969). *Philos. Mag.* **19**, 13–24.
Juers, D. H. & Matthews, B. W. (2001). *J. Mol. Biol.* **311**, 851–862.
Kakac, S., Shah, R. K. & Aung, W. (1987). *Handbook of Single-phase Convective Heat Transfer.* New York: John Wiley.
Kiefersauer, R., Than, M. E., Dobbek, H., Gremer, L., Melero, M., Strobl, S., Dias, J. M., Soulimane, T. & Huber, R. (2000). *J. Appl. Cryst.* **33**, 1223–1230.
Kramers, H. (1946). *Physica*, **12**, 61–80.
Kriminski, S., Caylor, C. L., Nonato, M. C., Finkelstein, K. D. & Thorne, R. E. (2002). *Acta Cryst.* D**58**, 459–471.
Krokida, M. K., Michailidis, P. A., Maroulis, Z. B. & Saravacos, G. D. (2002). *Int. J. Food Prop.* **5**, 63–111.
Kurinov, I. V. & Harrison, R. W. (1995). *Acta Cryst.* D**51**, 98–109.

Kuzay, T. M., Kazmierczak, M. & Hsieh, B. J. (2001). *Acta Cryst.* D**57**, 69–81.
Landau, L. D. & Lifshitz, E. M. (1986). *Theory of Elasticity*. Oxford University Press.
Landau, L. D. & Lifshitz, E. M. (1987). *Fluid Mechanics*. Oxford University Press.
Liakhovski, D. N. (1940). *Zh. Tekh. Fiz.* **10**, 999–1013.
Lide, D. R. (2000). Editor. *CRC Handbook of Chemistry and Physics*. Boca Raton, FL, USA: CRC Press.
Lomakin, A., Asherie, N. & Benedek, G. B. (1999). *Proc. Natl Acad. Sci. USA*, **96**, 9465–9468.
Mayer, E. (1985). *J. Microsc.* **140**, 3–15.
Mayer, E. (1988). *Cryo-Lett.* **9**, 66–77.
Miyazaki, Y., Matsuo, T. & Suga, H. (2000). *J. Phys. Chem. B*, **104**, 8044–8052.
Moffat, K. (1989). *Annu. Rev. Biophys. Biophys. Chem.* **18**, 309–332.
Morozov, V. N. & Gevorkian, S. G. (1985). *Biopolymers*, **24**, 1785–1799.
Morozov, V. N. & Morozova, T. Y. (1993). *J. Biomol. Struct. Dyn.* **11**, 459–481.
Nave, C. (1995). *Radiat. Phys. Chem.* **45**, 483–490.
Nicholson, J., Nave, C., Fayz, K., Fell, B. & Garman, E. (2001). *Nucl. Instrum. Methods Phys. Res. A*, **467**, 1380–1383.
Peyrard, M. (2001). *Phys. Rev. E*, **6401**, 1109–1114.
Rah, K. & Eu, B. C. (2001). *J. Chem. Phys.* **114**, 10436–10447.
Ranz, W. E. & Marshall, W. R. (1952*a*). *Chem. Eng. Prog.* **48**, 141–146.
Ranz, W. E. & Marshall, W. R. (1952*b*). *Chem. Eng. Prog.* **48**, 173–180.
Rastorguev, Y. L. & Ganiev, Y. A. (1966). *Russ. J. Phys. Chem.* **40**, 869-and.
Renksizbulut, M. & Yuen, M. C. (1983). *J. Heat Transfer*, **105**, 389–397.
Rodgers, D. W. (1994). *Structure*, **2**, 1135–1140.
Rohsenow, W. M., Hartnett, J. P. & Ganic, E. N. (1985). *Handbook of Heat Transfer Applications*. New York: McGraw–Hill.
Roles, K. A. & Wunderlich, B. (1991). *Biopolymers*, **31**, 477–487.
Ryan, K. P. (1992). *Scanning Microsc.* **6**, 715–743.
Sartor, G., Hallbrucker, A., Hofer, K. & Mayer, E. (1992). *J. Phys. Chem.* **96**, 5133–5138.
Sartor, G., Hallbrucker, A. & Mayer, E. (1995). *Biophys. J.* **69**, 2679–2694.
Sartor, G. & Mayer, E. (1994). *Biophys. J.* **67**, 1724–1732.
Sartor, G., Mayer, E. & Johari, G. P. (1994). *Biophys. J.* **66**, 249–258.
Schlichting, H. (1979). *Boundary Layer Theory*. New York: McGraw–Hill.
Sharpe, L. & Morrison, F. A. (1986). *J. Heat Transfer*, **108**, 337–342.
Slack, G. A. (1980). *Phys. Rev. B*, **22**, 3065–3071.
Snell, E. H., Judge, R. A., Larson, M. & van der Woerd, M. J. (2002). *J. Synchrotron Rad.* **9**, 361–367.
Speziale, S., Jiang, F., Caylor, C. L., Kriminski, S., Zha, C.-S., Thorne, R. E. & Duffy, T. S. (2003). In the press.
Steinrauf, L. K. (1959). *Acta Cryst.* **12**, 77–79.
Sutton, R. L. (1991*a*). *J. Chem. Soc. Faraday Trans.* **87**, 3747–3751.
Sutton, R. L. (1991*b*). *J. Chem. Soc. Faraday Trans.* **87**, 101–105.
Teng, T. Y. (1990). *J. Appl. Cryst.* **23**, 387–391.
Teng, T. Y. & Moffat, K. (1998). *J. Appl. Cryst.* **31**, 252–257.
Tilton, R. F., Dewan, J. C. & Petsko, G. A. (1992). *Biochemistry*, **31**, 2469–2481.
Tritton, D. J. (1988). *Physical Fluid Dynamics*. Oxford University Press.
Vyrubov, D. N. (1939). *Zh. Tekh. Fiz.* **9**, 1923–1931.
Walker, L. J., Moreno, P. O. & Hope, H. (1998). *J. Appl. Cryst.* **31**, 954–956.
Weik, M., Kryger, G., Schreurs, A. M. M., Bouma, B., Silman, I., Sussman, J. L., Gros, P. & Kroon, J. (2001). *Acta Cryst.* D**57**, 566–573.
Whitaker, S. (1972). *AICHE J.* **18**, 361–371.
White, F. M. (1991). *Viscous Fluid Flow*. New York: McGraw–Hill.
Wong, K. L., Lee, S. C. & Chen, C. K. (1986). *J. Heat Transfer*, **108**, 860–865.
Wukovitz, S. W. & Yeates, T. O. (1995). *Nature Struct. Biol.* **2**, 1062–1067.
Xu, X., Jeronimidis, G., Atkins, A. G. & Trusty, P. A. (2003). *J. Mater. Sci.* **38**, 245–253.
Yang, P. H. & Rupley, J. A. (1979). *Biochemistry*, **18**, 2654–2661.
Young, A. C. M., Tilton, R. F. & Dewan, J. C. (1994). *J. Mol. Biol.* **235**, 302–317.
Young, R. D., Frauenfelder, H., Johnson, J. B., Lamb, D. C., Nienhaus, G. U., Philipp, R. & Scholl, R. (1991). *Chem. Phys.* **158**, 315–327.
Yuge, T. J. (1960). *J. Heat Transfer*, **82**, 214–220.
Zasadzinski, J. A. N. (1988). *J. Microsc.* **150**, 137–149.